

Study of galaxy morphology and merging time of two interacting galaxies under different initial rotation and orientation configurations

Elkin L. López*, Gustavo V. López†, Simon N. Kemp ‡

Departamento de Física, Universidad de Guadalajara,
Blvd. Marcelino García Barragan y Calzada Olímpica,
CP 44200, Guadalajara, Jalisco, México,

‡Instituto de Astronomía y Meteorología, Universidad de Guadalajara,
Av Vallarta 2602, Col Arcos Vallarta,
CP 44130, Guadalajara, Jalisco, México,

February 20, 2024

Abstract

Using the GADGET-2 N-body code, we make a study of the galaxy morphology and merging time due to two interacting galaxies (for the same types and different sizes and masses, 1 : 1 and 1 : 10 ratio masses) merging due to gravity interaction. This is done for different initial relative orientation and rotation of these galaxies (modes of interaction) but with the same relative bulge separation and the same relative initial velocities. It was found that the resulting galaxy morphology resemble many of the observed galaxies in our Universe, and that, in general, a binary galaxy system with 1:10 mass ratio has larger merging time than a binary galaxy system with 1:1 mass ratio. This difference is due to the different evolution of the masses during the interaction in both cases. For the case with a 1:10 mass ratio, the global mass maximum is located at the end evolution, meaning that the second galaxy increases its mass constantly. For the case with mass ratio 1:1, the global maximum is located around $t = 0.35$ Gy, causing a reduction of the merging time.

Keywords: galaxies: kinematics and dynamics, galaxies: interactions, galaxies: bulges, galaxies: binary

PACS: 98.35.Gi, 98.35.Jk, 9865.At, 98.65.Fz

*lopezlopezelkin@gmail.com

†gulopez@cencar.udg.mx

‡snk@astro.iam.udg.mx

1 Introduction

The interaction of two galaxies is a very common process in our Universe (Larson & Tinsley, 1978), and the observed galaxy morphology of the merger product depends on the time after the initial encounter in which it is observed (Boylan-Kolchin M. & E., 2008, Koyama, 2019). At the end of the interaction we may have a ‘new’ galaxy with different bulge and disk components and different distributions of gas, dust, and stars (Karademir et al., 2019, Moody C.E. & J.R., 2014, Wuyts S. & N.M.F., 2009). It is of interest to know the differences in the resulting galaxy morphology and the merging time for different initial orientations of both galaxies, the size and mass of the resultant bulge/ellipsoid and disk components, and the different distributions of gas and stars in the final merger product.

There have been many studies of simulations of the interaction of two galaxies (Moreno et al., 2019, Pontzen et al., 2016, Wallin et al., 2016) mapping the exchange of gas and stars (Besla G., 2012, Hopkins P.F., 2013). Karademir et al. (2019) studied the distribution of deposition of mass via minor mergers ($\mu = 0.1 - 0.25$) and mini mergers ($\mu = 0.01 - 0.1$) finding that mini mergers deposit a larger fraction of the stars in the exterior parts of the galaxy compared with minor mergers and do not contribute much to the central mass. Mini mergers can increase the size of the main disk component significantly. The find that streams result from circular satellite orbits while shells form from more radial orbits. Kim & Ostriker (2018) investigate the formation of warped disks of spiral galaxies in ‘fly-by’ encounters of these galaxies with adjacent dark matter haloes, finding that such encounters can produce warps that last several Gigayears. However, as far as we know, there has no been a systematic study of this interaction with all possible basic orientation of galaxies. Here we present a systematic study of the galaxy morphology and merging time of two interacting galaxies with different orientations of their rotation axes and different sense of rotation of the disk. We use the GADGET-2 N-body code (Springel, 2005, Springel et al., 2005, Springel & White, 1999) considering different relative orientations and rotation. The galaxies are initially at the same separation and have the same relative velocity and we start the orbit of the second galaxy in the tangential direction.

2 Configurations

We consider two symmetrical fried-egg-shaped galaxies with bulge (Bertin, 2000, Bouwens et al., 1999, Dwek et al., 1995, Launhardt et al., 2002, Milosavljević & Merritt, 2001, Salviander et al., 2007, Xu et al., 2007) and disk components (Bertin, 2000, Burkert et al., 1992, Giallongo et al., 2000, Kennicutt Jr., 1983, Kennicutt Jr. et al., 1987, van der Kruit, 2010) containing stars, gas, and dust (Bertin, 2000, Daylan et al., 2016, Ivison et al., 2010, Kacprzak et al., 2011), plus a dark matter halo (Bode et al., 2001, Oppenheimer et al., 2001). The centre of the bulge defines the trajectory of the galaxy (Holtzman et al., 1998, Magorrian et al., 1998), which usually coincides with the centre of the dark matter halo (Wechsler & Tinker, 2018). Galaxies exist in binary systems and in small groups (less than 100 members) or large clusters of galaxies (Gallagher III & Ostriker, 1972, Paul & Gupta, 2017, Turner, 1976, Voit, 2005).

We will adopt the following convention for the initial configuration of the two galaxies with respect to the Cartesian reference system: (a) If the plane of the galaxy’s disk is in the x-y plane of the system and it is rotating in a counter-clockwise direction, we denote it as Z^+ (axis of rotation). If this galaxy is rotating in a clockwise direction, we denote it as Z^- . (b) If the plane of the galaxy’s is in the x-z plane of the reference system and is rotating in a counter-clockwise direction, we denote it as Y^+ (axis of rotation), and for its clockwise direction as Y^- . (c) If the plane of the galaxy’s disk is in the z-y plane of the reference system, we denote it as X^+ for the counter-clockwise direction of rotation, and X^- for the clockwise direction. For each galaxy we therefore consider six cases, and so we have a total of 36 possible combinations of orientation and rotation of the two galaxies in the interaction: (Z^+, Z^+) , (Z^+, X^+) , \dots , (Z^-, X^-) . In addition, we consider two mass relations: (a) when the central (primary) galaxy is ten times the mass of the orbiting (secondary) galaxy, (b) when they are of equal masses. To denote the interaction configuration of the pair we then use

a pair of terms, the first term is the primary galaxy's rotation state, and the second term is the secondary galaxy's rotation state.

Figure 1 shows the initial positions for (Z^+, X^+) and (Z^+, Y^+) , having different masses. In all cases under our consideration, the galaxies will have the same distance separation at the beginning of the simulation.

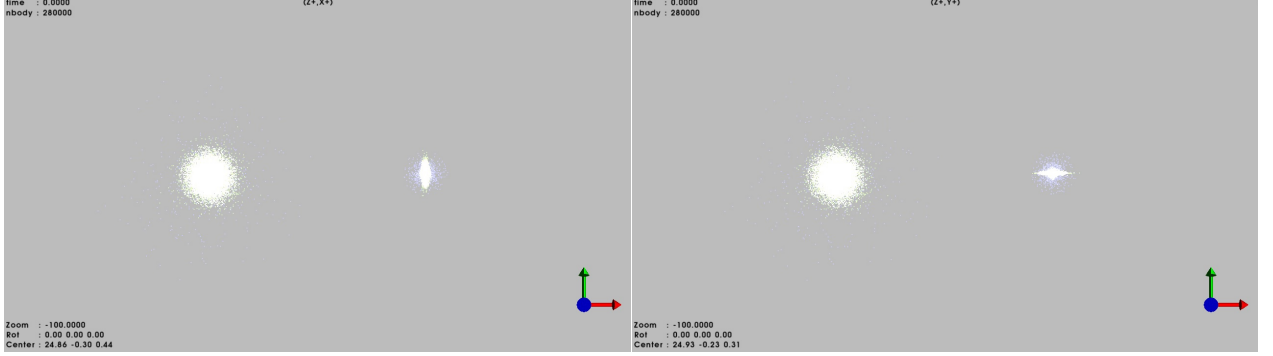


Figure 1: Two interacting galaxies with different modes; (Z^+, X^+) on the left and (Z^+, Y^+) on the right

3 Simulations

We use our available version of the GADGET-2 N-body code to make the simulations of the interactions mentioned above. Details of this code can be found in the above mentioned references, but we want to state some important characteristics used in our simulations. If r_{200} is the radius containing three-quarters of the galaxy mass, where the density is 200 times the critical density of the universe and v_{200} is the rotation velocity or velocity dispersion at this radius, then the total mass of the galaxy within this radius is $M_{200} = v_{200}^2 r_{200} / G$, where G is the gravitational constant ($G = 6.674 \times 10^{-11} \text{ m}^3 \text{ kg}^{-1} \text{ s}^{-2}$, Rose et al. (1969)).

$$M_{200} = M_{bulge} + M_{halos} + M_{disk}. \quad (1)$$

The halo and bulge densities, as a function of the radius (r) of the galaxy, are

$$\rho_{halo,bulge}(r) = \frac{M_{halo,bulge}}{2\pi} \frac{a_{h,b}}{r(r + a_{h,b})^3}, \quad (2)$$

where the parameter $a_{h,b}$, in terms of the concentration index c , is $a_h = r_s \sqrt{2[\ln(1+c) - c/(1+c)]}$, and the halo scale length is defined as $r_s = r_{200}/c$ and the proportion bulge scale length per scale radius $f_b = a_b/R_d$, where R_d is the scale length of the disk. The angular momentum of the halo is

$$J = \lambda \sqrt{2GM_{200}^3 r_{200} / f_c}, \quad (3)$$

where λ is the twist parameter, and the parameter f_c , written in terms of the concentration index, is $f_c = c[1 - 1/(1+c)^2 - 2\ln(1+c)/(1-c)] / (2[\ln(1+c) - c/(1+c)]^2)$. The fractional angular momentum of the bulge is $J_b = JM_{bulge}/M_{200}$, and the angular momentum of the disk is $J_d = j_d J$, j_d being a free parameter. The disk (stellar) density varies as

$$\rho_*(R, z) = \frac{M_*}{4\pi z_0 R_d^2} \text{sech}^2\left(\frac{z}{z_0}\right) \exp\left(-\frac{R}{R_d}\right), \quad (4)$$

where $R = \sqrt{x^2 + y^2}$, z_0 is the parameter which determines the thickness of the disk, and M_* is the stellar mass on the disk. Similarly, the gas in the disk has a surface density of

$$\Sigma_{gas} = \frac{M_{gas}}{2\pi h_r^2} \exp\left(-\frac{r}{h_r}\right), \quad (5)$$

where h_r is the scale length of the gas profile, and $M_{gas} + M_* = M_{disk}$. In addition, the vertical structure of gas in asymmetric galaxies is governed by the equation

$$\frac{1}{\rho_{gas}} \frac{\partial P}{\partial z} + \frac{\partial \Phi}{\partial z} = 0, \quad (6)$$

where Φ is the gravitational potential due to the total mass of the gas.

Our simulation of two interacting galaxies with the GADGET-2 code were performed with the following set of parameters for the primary galaxy G_1 and the secondary galaxy G_2 (N_i being the number of elements of each part of the galaxy):

G_1 :

$$\begin{array}{llllll} c = 10.0, & v_{200} = 120 \text{ km/s}, & R_d = 1.04722 \text{ h}^{-1}\text{kpc}, & \lambda = 0.033, & M_d/M_{200} = 0.04, \\ M_b/M_{200} = 0.09, & M_{gas}/M_d = 0.1, & a_b/R_d = 0.2, & z_0/R_d = 0.2, & J_d/J = 0.04, \\ N_{halo} = 150,000, & N_{disk} = 20,000, & N_{gas} = 20,000, & N_{bulge} = 10,000. \end{array}$$

G_2 :

$$\begin{array}{llllll} c = 10.0, & v_{200} = 55.699 \text{ km/s}, & R_d = 0.486075 \text{ h}^{-1}\text{kpc}, & \lambda = 0.033, & M_d/M_{200} = 0.04, \\ M_b/M_{200} = 0.09, & M_{gas}/M_d = 0.1, & a_b/R_d = 0.2, & z_0/R_d = 0.1, & J_d/J = 0.04, \\ N_{halo} = 30,000, & N_{disk} = 20,000, & N_{gas} = 20,000, & N_{bulge} = 10,000. \end{array}$$

The initial conditions of our two galaxies for all modes of interaction are: $\vec{x}_1 = \vec{0} \text{ h}^{-1}\text{kpc}$, $\vec{x}_2 = 50\hat{x} \text{ h}^{-1}\text{kpc}$ ($h = H_0/100 \text{ km s}^{-1} \text{ Mpc}^{-1}$ observationally $h \sim 0.7$ and $1 \text{ kpc} \approx 206264806 \text{ AU}$ with $1 \text{ AU} \approx 149.6 \times 10^6 \text{ km}$), the velocities are $\vec{v}_1 = \vec{0} \text{ km/s}$ and $\vec{v}_2 = 99.0548172\hat{y} \text{ km/s}$. The subindex 1 represents the primary galaxy and 2 represents the secondary one. The baryonic masses of the galaxies are $\mathcal{M}_1 = 57.4 \times 10^{10} M_\odot$ and $\mathcal{M}_2/\mathcal{M}_1 = 0.1, 1$ (for 1:10 and 1:1 mass ratios respectively).

We define the merging time (illustrated in Figure 2 and 9) as the time where the asymptotic behavior of the galaxies' separation and oscillations in separation reach defined limits, as a consequence of the fusion of the bulges. This time is calculated in the following way: given a small $\epsilon \in \mathbb{R}$, we can find a time t_ϵ , such that for any $t > t_\epsilon$, we have $|\dot{d}(t > t_\epsilon)| / |d(0)/\Delta t| \leq \epsilon$, and at the time t_ϵ we have $|\dot{d}(t_\epsilon)| / |d(0)/\Delta t| > \epsilon$. Thus, time t_ϵ marks the division between oscillations of high amplitude ($t \leq t_\epsilon$) and oscillations of small amplitude ($t > t_\epsilon$). The merging time τ is defined as $\tau = t_\epsilon + q\Delta t$, where q is the smallest positive integer that satisfies that τ is the closest time to t_ϵ that satisfies $|\dot{d}(\tau)| / |d(0)/\Delta t| \approx 0$. For this estimation we used the following parameters: $\epsilon = 0.004$ and $d(0)/\Delta t = 5000 \text{ kms}^{-1}$ with $\Delta t = 0.01 \text{ (0.98 h}^{-1}\text{Gyr)}$.

The resulting galaxy morphology of the two galaxies interaction at the final time t_f of our simulation will be characterized by the resulting parameters $M_*(t_f)$, $R_d(t_f)$, and $z_0(t_f)$. Although we also present the shape of the merged galaxy in different planes at different times.

4 Results

4.1 Galaxies interaction for $M_2 = M_1/10$

Figure 2 shows the evolution of the distance between the centres of the galaxies' bulges for all 36 interaction modes (rotation, orientation) of the galaxies with mass ratio 1:10. There are six groups of 6 modes each (each group for a color), and in each group the primary galaxy has the same rotation and orientation mode. Each group has similar evolution of the separation during the interaction, indicating the behaviour is dominated by the the primary galaxy.

As imentioned above, the merging time is defined as when the oscillations in separation of the centres reach a determined minimum level (when the velocity derivative of the curve tends to zero). The merging time τ of the galaxies is shown in the second column of Table 1 for different masses (first number). The merging time for different masses is quicker for the Z^+ cases and slowest for the Z^- cases. For Z^+ the primary galaxy is rotating in the same direction and in the same orbital plane as the orbital movement of the secondary galaxy, meaning that the stars are in closer contact for a longer time and so have more time to interact. The Z^- cases have the longest merger time because the primary galaxy is rotating in the opposite direction to the orbital motion of the secondary galaxy. The rotating direction of the secondary galaxy has relatively little effect on the merging times.

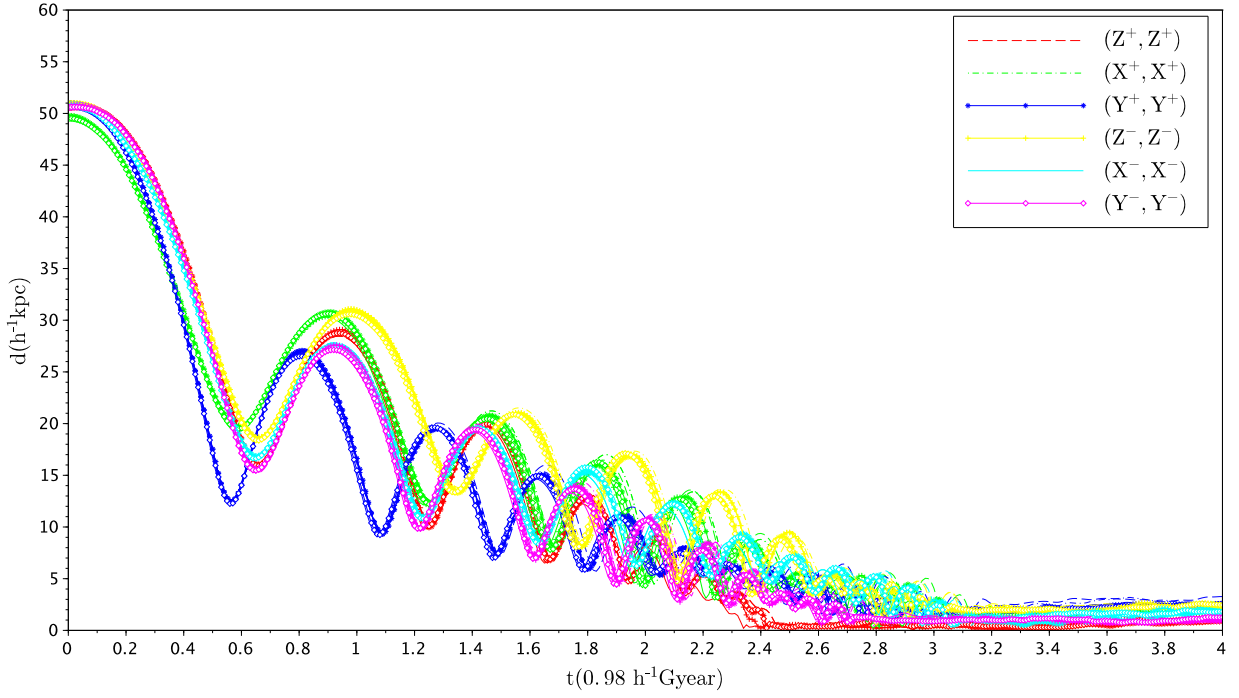


Figure 2: Time evolution of the separation of the centres of the bulges of two interacting galaxies for 36 modes.

Figures 3–8 show the galaxy morphologies and position of stars of the two galaxies, at time $t = 0.0, 2.0, 4.0$ ($0.98 \text{ h}^{-1} \text{ Gyr}$), for all rotation and orientation interaction modes (36 modes) and for the mass ratio 1:10. These modes of interaction take a long time, and even at 4 Gyr the merged galaxy looks like a disk galaxy with bulge and, often, with a distorted antisymmetrical disk. This disk is frequently extended in agreement with Karademir et al. (2019). At the time 2 Gyr, there are structures which look like arcs in shell galaxies but in the plane of the disk, and their formation from a companion with tangential orbits, in contradicts the results of Karademir et al. (2019). We note that this interaction configuration favours the formation of disk galaxies as a final merger product, as the tangential orbits of the secondary galaxy gives a high initial angular momentum to the system, which tends to remian in the disk component of the final product.

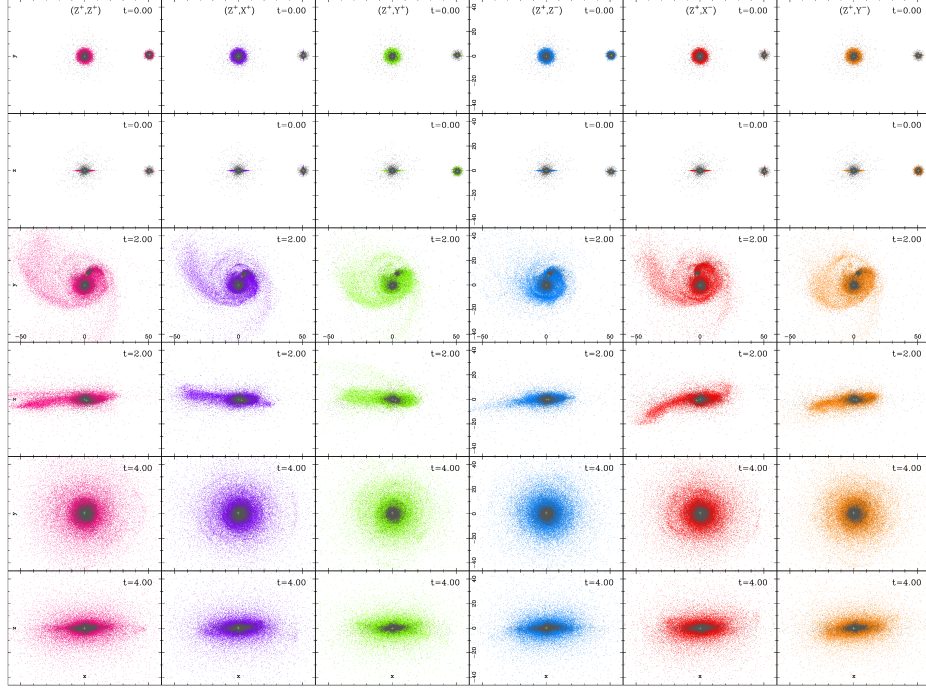


Figure 3: Bulge stars in grey and disk stars coloured, for all interactions of mass ratio 1:10 with mode Z^+ , each column showing one mode of interaction. The initial configuration $t = 0.0$ Gyr (top), $t = 2.0$ Gyr (middle), $t = 4.0$ Gyr (bottom) . Each time has two perspectives, the x-y plane and x-z plane, one above the other.

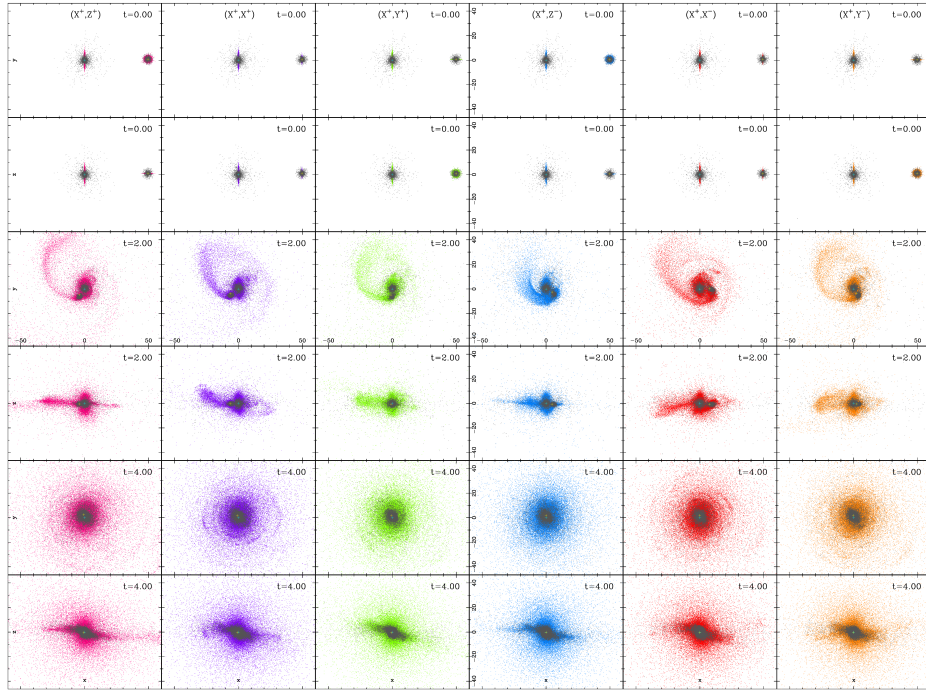


Figure 4: As Fig. 3 for all interactions with mass ratio 1:10 in which rotation of the primary galaxy is X^+

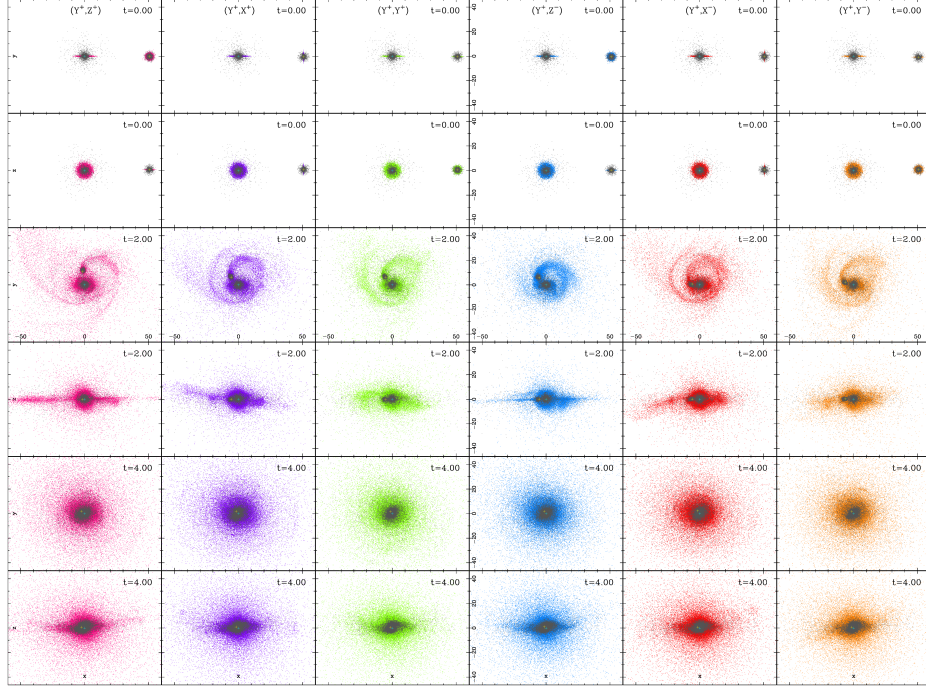


Figure 5: As Fig. 3 for all interactions with mass ratio 1:10 in which the rotation of primary galaxy is Y^+

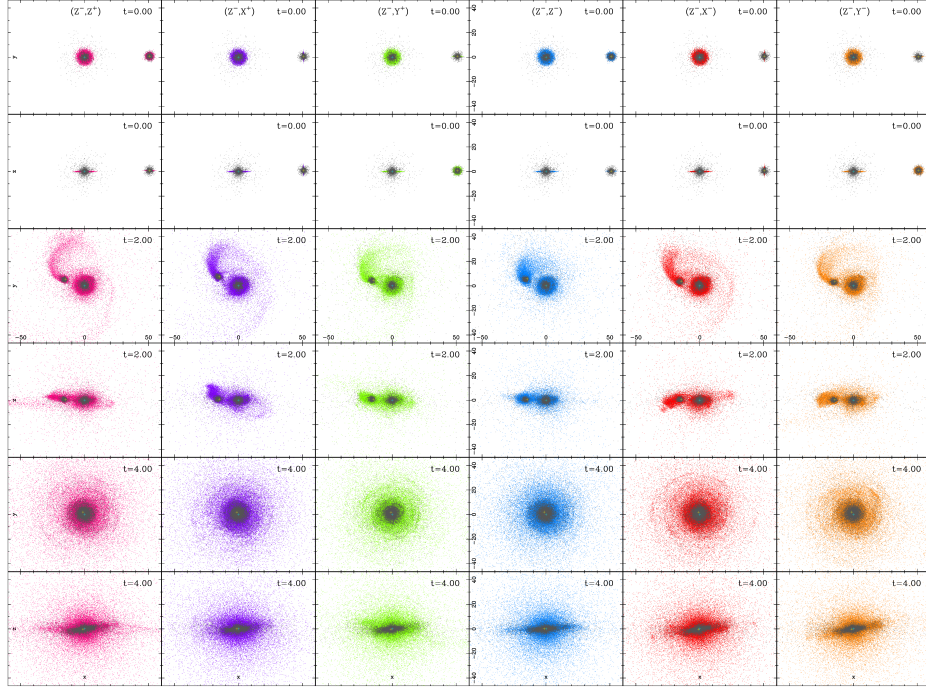


Figure 6: As Fig. 3 for all interactions with mass ratio 1:10 in which rotation of the primary galaxy is Z^- .

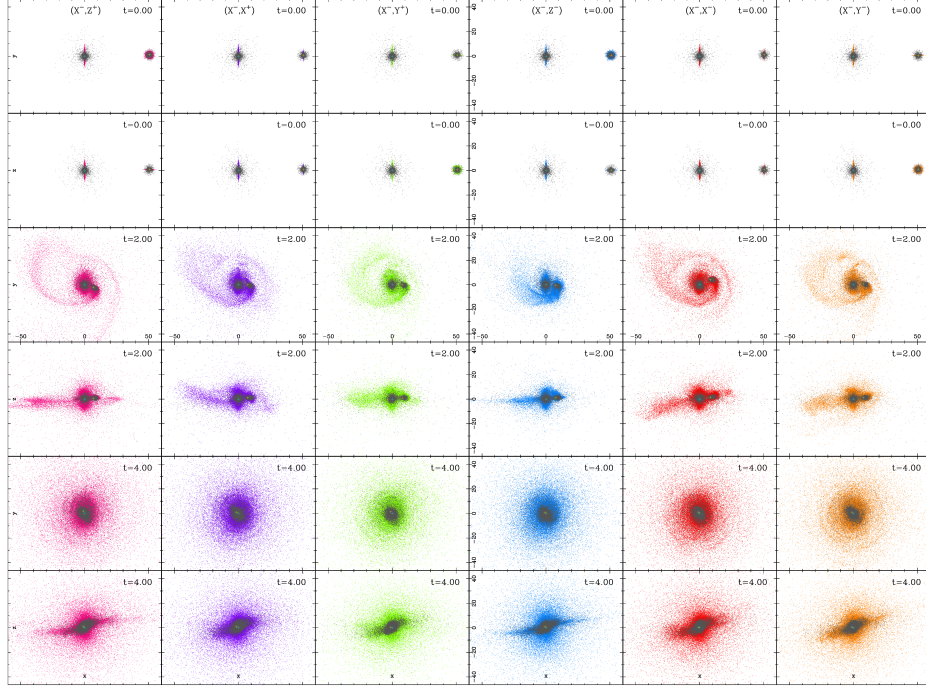


Figure 7: As Fig. 3 for all interactions with mass ratio 1:10 in which the rotation of primary galaxy is X^-

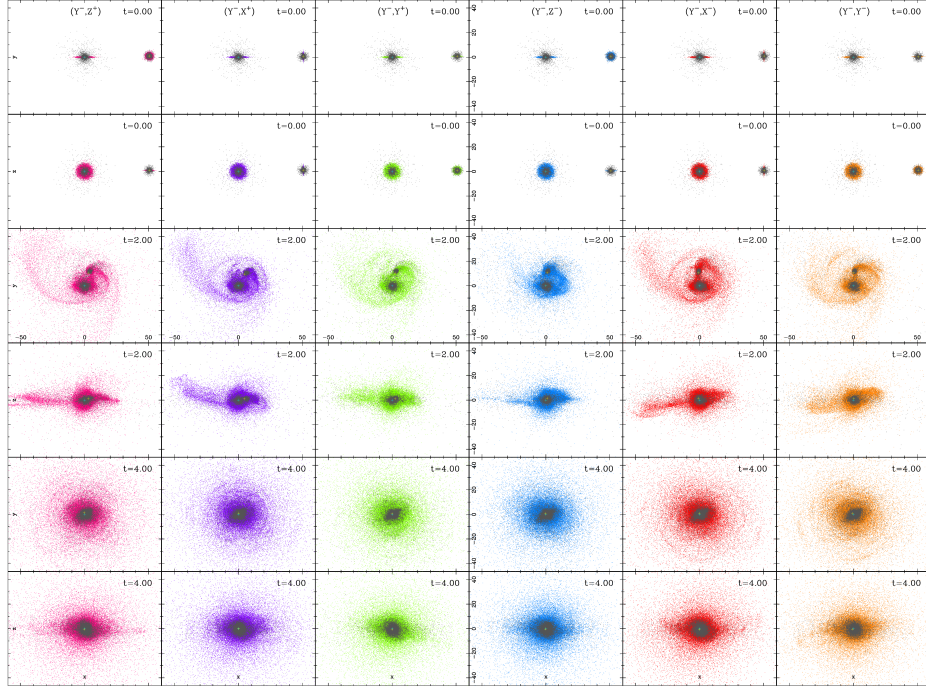


Figure 8: As Fig. 3 for all interactions with mass ratio 1:10 in which the rotation of primary galaxy is Y^- .

4.2 Galaxies interaction for $M_2 = M_1$

We consider now that the second galaxy has the same parameters as the first one, and we repeat all the cases we had before. Figure 9 shows the evolution of distance of separation of the galaxies' bulges for all interaction modes. The merging time τ is shown in the second column (second number) of Table 1. With the secondary galaxy having much more mass, the fusion times are much shorter, between 0.5–0.7 ($0.98 \text{ h}^{-1}\text{Gyr}$), depending on if they are considered to be merged on the second or third close encounter.

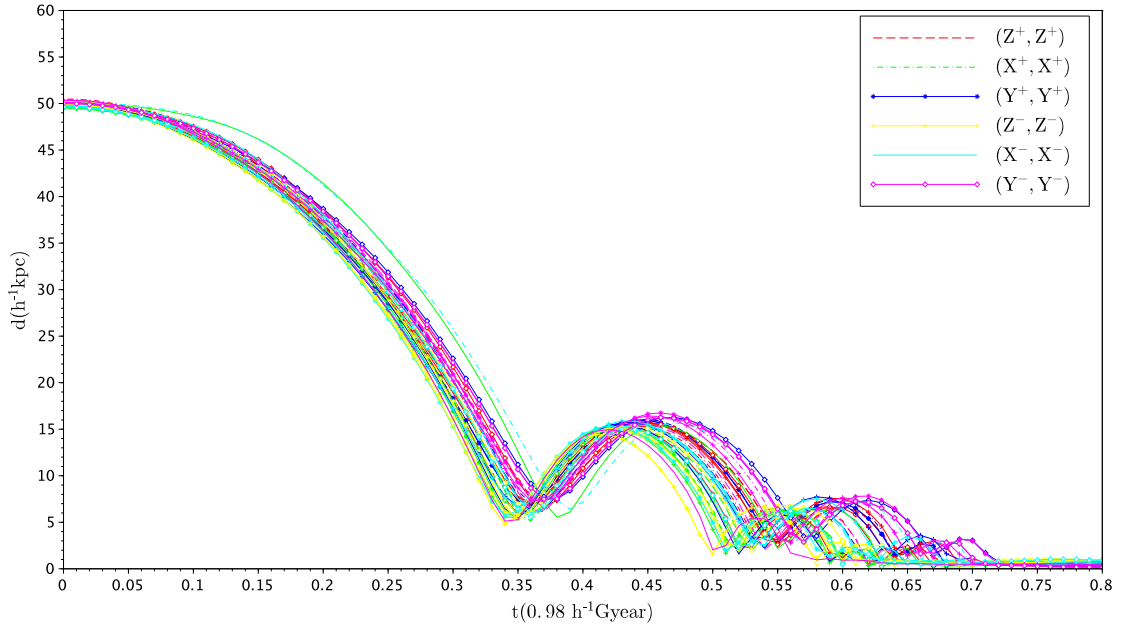


Figure 9: Time evolution of the separation of the bulges of two interacting galaxies for 36 modes.

Figures 10-15 show the galaxy morphologies and the positions of galaxy stars at times $t = 0.0, 0.5, 1.0$ ($0.98 \text{ h}^{-1}\text{Gyr}$), top to bottom in each column, for all rotation interaction modes (36 modes). The time intervals between frames are shorter because the merging process is more rapid in this case. Here the intermediate and final-stage disks are not as extended as in the 1:10 mass ratio cases, as expected for equal-mass mergers Karademir et al. (2019) and the arc-like structures in the disk plane in the final stage look more like sections of spiral arms than shell structures. The cases with the secondary galaxy in the rotation state Z^+ all finish with a disturbed, asymmetric, warped disk, while Z^+, Z^+ is more regular with a box-peanut-like bulge. The other orientations seem more dominated by the galaxy morphology of the bulge/ellipsoid in the final stage, again some of these are box-peanut-like. In this case, with the secondary galaxy as massive as the first, the initial angular momentum of the system is even higher when the secondary galaxy is in the Z^+ rotation state, favouring the formation of an extended disk structure. If the secondary galaxy is another rotation state the final merger product is more elliptical-like.

Figure 16 shows a comparison of two different visualizations of the (X^+, Z^-) interaction for mass ratio 1:10 at time $t = 4.0$ ($0.98 \text{ h}^{-1}\text{Gyr}$), the left hand side shows all baryonic galaxy stars and the right hand side shows only the disk stars of the galaxy. It can be seen that the initial disk stars spread out and some form part of the bulge of the merger product. Both images are similar but there are more stars further from the plane above and below the bulge in the image with all galaxy stars. the same angled, rather distorted disk is seen in both.

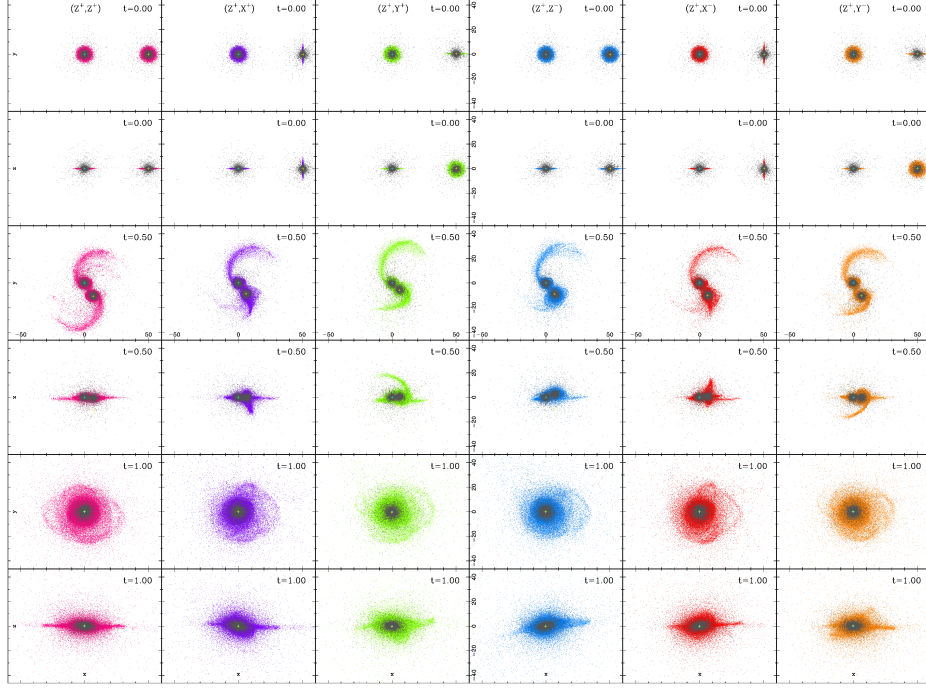


Figure 10: Bulge stars in grey and disk stars coloured, for all interactions of mass ratio 1:1 in which the rotation of the primary galaxy is Z^+ , a mode by column (color). The initial configuration at $t = 0.0$ Gyr (top), $t = 0.5$ Gyr in middle, $t = 1.0$ Gyr in the bottom. Each time has two perspectives, x-y plane and x-z plane, one above the other.

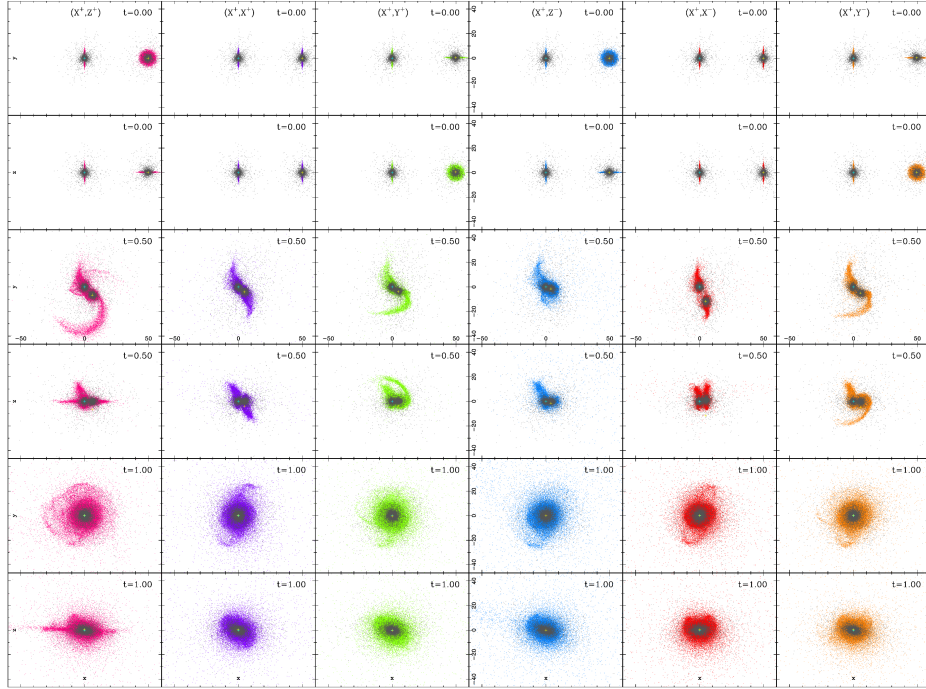


Figure 11: As Fig. 9 for all interactions with mass ratio 1:1 in which the rotation of primary galaxy is X^+ .

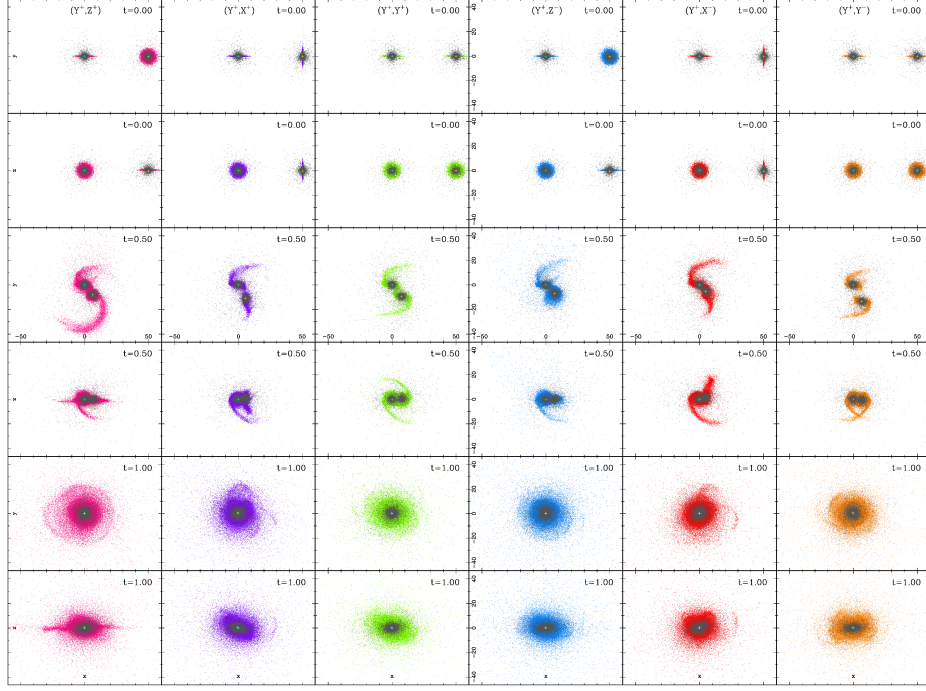


Figure 12: As Fig. 9 for all interactions with mass ratio 1:1 in which the rotation of primary galaxy is Y^+ .

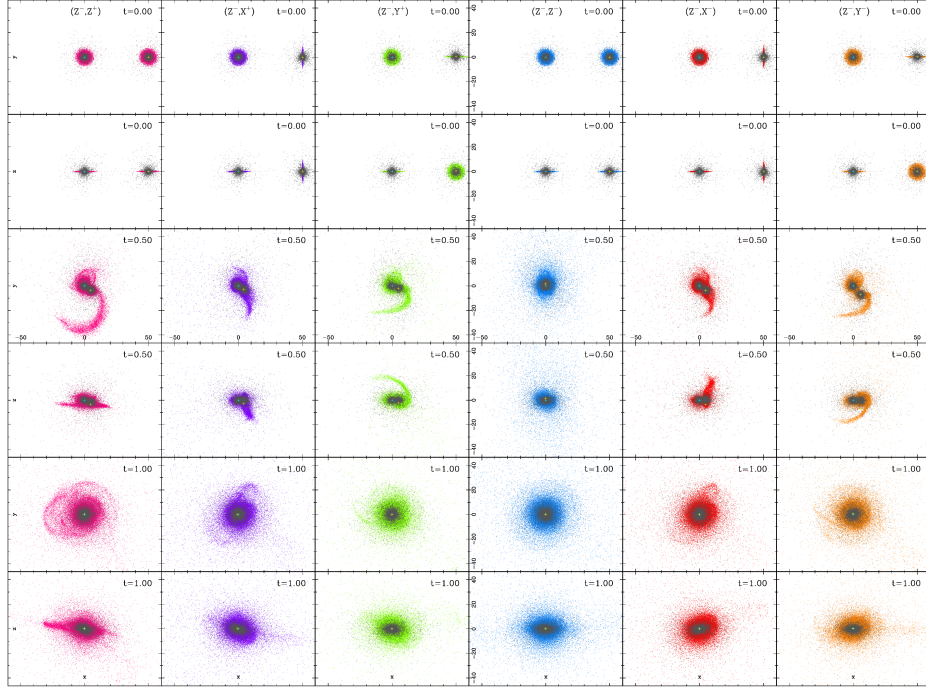


Figure 13: As Fig. 9 for all interactions with mass ratio 1:1 in which the rotation of primary galaxy is Z^- .

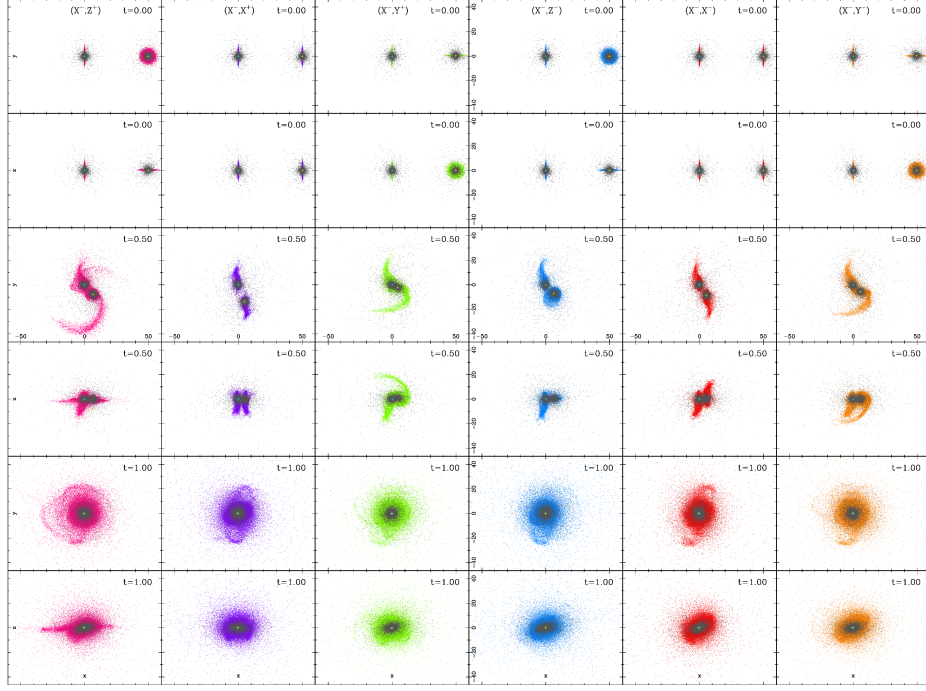


Figure 14: As Fig. 9 for all interactions with mass ratio 1:1 in which the rotation of primary galaxy is X^- .

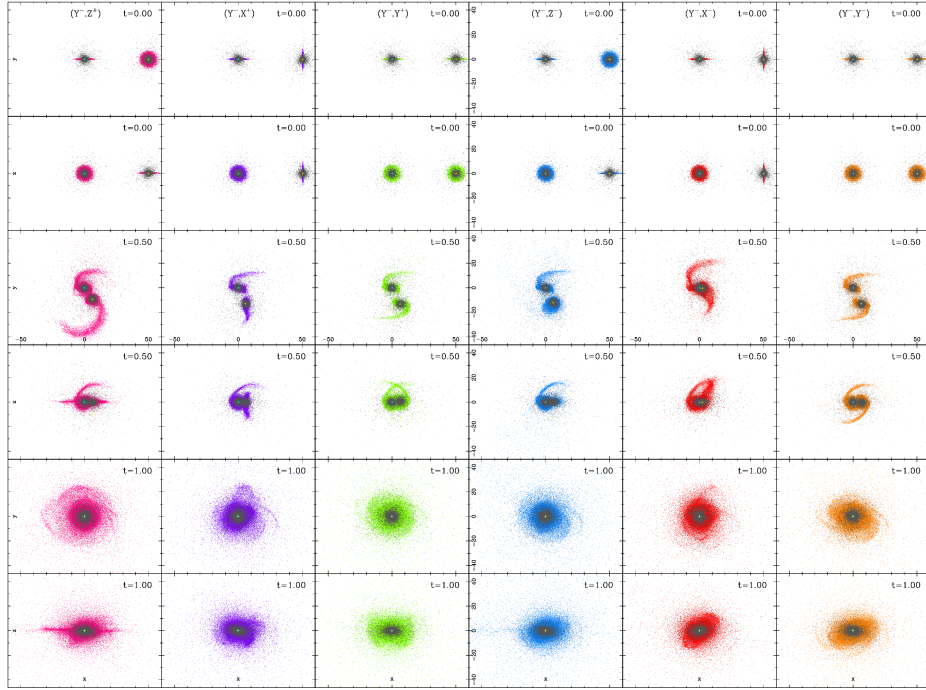


Figure 15: As Fig. 9 for all interactions with mass ratio 1:1 in which the rotation of primary galaxy is Y^- .

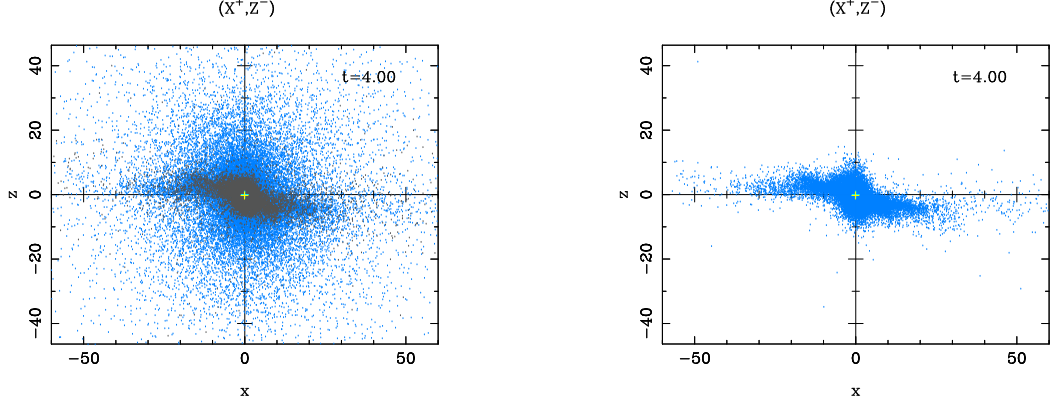


Figure 16: (X^+, Z^-) interaction for 1:10 ratio at time $t = 4.0$, the left side shows all galaxies stars and the right side the disks stars of the galaxies. The bulge stars are grey and the star and gas stars are blue.

4.3 Comparison

Table 1 shows the merging time (τ). In addition and at the time $t_f = 4$ ($0.98 \text{ h}^{-1}\text{Gyr}$, final time of the simulations), it is shown the stellar mass M_* (calculated from the mass $\mathcal{M}(R_d, z_0)$ of a cylinder of radius R_d), the scale length of the disk R_d (calculated using the cylinder method explained below), and the scale height z_0 . Values of $M_*(0)$, $R_d(0)$ and $z_0(0)$ are initial parameters of the primary disk (G_1 at time $t = 0$). The proportions in columns 4, 5 and 6 indicate how much the disk is taller, more extended or more massive, compared with the initial disk of the primary galaxy. In each column the number on the left is the result for the mass ratio 1:10 and the number on the right is the result for the mass ratio 1:1, shown together for ease of comparison.

Cylinder method; For all modes of 1:10 and most cases of 1:1, (no matter orientation nor rotation) we see a new bigger disk in the orbit plane (X-Y) because the orbital momentum dominates. This ‘new disk’ is analysed using the volume integration of equation (4). This is,

$$\mathcal{M}(R, z) = M_* \tanh\left(\frac{z}{z_0}\right) \left[1 - \left(1 + \frac{R}{R_d}\right) \exp\left(-\frac{R}{R_d}\right)\right], \quad (7)$$

where $\mathcal{M}(R, z)$ is the mass inside a cylinder of radius R and height $2z$ (the height of the cylinder is in the Z-direction for all the 36 cases for mass ratios 1:10 and 1:1). To determine the values of R_d , z_0 and M_* at time t , we measure the mass of two cylinders of the same height z_r and different radii r_1 and r_2 ($r_1 < r_2$) at time t , using equation (7) to get the fractional mass $f_r = \mathcal{M}(R_1, z_r)/\mathcal{M}(R_2, z_r)$ that satisfies

$$f_r \left[1 - \left(1 + \frac{R_2}{R_d}\right) \exp\left(-\frac{R_2}{R_d}\right)\right] = 1 - \left(1 + \frac{R_1}{R_d}\right) \exp\left(-\frac{R_1}{R_d}\right). \quad (8)$$

Then, we measure the mass of two cylinders of the same radius R_h and different heights z_1 and z_2 ($z_1 < z_2$) at time t , using equation (7) to get the fractional mass $f_h = \mathcal{M}(R_h, z_1)/\mathcal{M}(R_h, z_2)$ that satisfies

$$f_h \tanh\left(\frac{z_2}{z_0}\right) = \tanh\left(\frac{z_1}{z_0}\right). \quad (9)$$

It is necessary to explain that the cylinders used in this method have their centres in the primary bulge’s centre of mass at the time t (after the fusion). The equations (8) and (9) were solved numerically to obtain

R_d and z_0 at time t . From equation (7) for $R = R_d$ and $z_0 = z_0$ we have

$$\mathcal{M}(R_d, z_0) = \frac{M_*}{(1 - 2e^{-1}) \tanh(1)}, \quad (10)$$

Measuring the mass inside the cylinder $\mathcal{M}(R_d, z_0)$ we can calculate the stellar mass M_* .

Mode	τ (0.98 h ⁻¹ Gyr)		M_* (10 ¹⁰ h ⁻¹ M _⊙)		$M_*(t_f)/M_*(0)$		$R_d(t_f)/R_d(0)$		$z_0(t_f)/z_0(0)$	
(Z ⁺ ,Z ⁺)	2.50	0.68	1.35	1.23	0.94	0.85	1.17	1.85	2.03	1.94
(Z ⁺ ,X ⁺)	2.45	0.70	1.20	1.13	0.83	0.78	1.15	1.51	2.02	2.05
(Z ⁺ ,Y ⁺)	2.42	0.67	0.98	1.00	0.68	0.69	1.13	1.42	1.57	1.98
(Z ⁺ ,Z ⁻)	2.43	0.75	1.18	1.16	0.82	0.80	1.19	1.46	1.71	2.19
(Z ⁺ ,X ⁻)	2.38	0.73	1.33	0.98	0.92	0.68	1.21	1.45	1.98	1.80
(Z ⁺ ,Y ⁻)	2.53	0.68	1.00	1.02	0.69	0.70	1.12	1.50	1.47	1.83
(X ⁺ ,Z ⁺)	3.26	0.68	0.48	1.33	0.33	0.92	0.92	1.47	1.99	2.32
(X ⁺ ,X ⁺)	3.08	0.66	0.56	0.99	0.39	0.68	0.96	1.34	2.35	1.98
(X ⁺ ,Y ⁺)	3.15	0.63	0.56	0.80	0.39	0.56	1.03	1.31	2.07	2.01
(X ⁺ ,Z ⁻)	3.02	0.63	0.62	1.06	0.43	0.73	0.95	1.32	2.61	2.04
(X ⁺ ,X ⁻)	2.95	0.72	0.54	0.79	0.38	0.55	0.96	1.19	2.20	2.31
(X ⁺ ,Y ⁻)	3.00	0.64	0.46	0.82	0.32	0.56	0.97	1.26	1.79	1.75
(Y ⁺ ,Z ⁺)	3.22	0.65	0.67	1.15	0.47	0.79	0.95	1.50	2.23	2.26
(Y ⁺ ,X ⁺)	2.97	0.74	0.42	0.78	0.29	0.54	0.94	1.29	1.71	2.19
(Y ⁺ ,Y ⁺)	2.88	0.71	0.43	1.18	0.30	0.82	0.93	1.46	2.02	2.52
(Y ⁺ ,Z ⁻)	2.96	0.74	0.48	1.04	0.33	0.72	0.98	1.31	1.99	2.22
(Y ⁺ ,X ⁻)	2.89	0.69	0.58	0.70	0.40	0.48	0.98	1.29	2.28	2.15
(Y ⁺ ,Y ⁻)	2.92	0.78	0.50	0.68	0.35	0.47	0.90	1.32	2.05	2.19
(Z ⁻ ,Z ⁺)	3.14	0.64	0.74	0.89	0.51	0.61	0.97	1.39	1.64	2.02
(Z ⁻ ,X ⁺)	3.13	0.65	0.74	0.74	0.51	0.51	0.99	1.33	1.57	1.75
(Z ⁻ ,Y ⁺)	3.00	0.69	0.80	0.87	0.55	0.60	1.01	1.31	1.75	2.20
(Z ⁻ ,Z ⁻)	3.02	0.66	0.77	1.16	0.53	0.80	1.02	1.37	1.69	2.18
(Z ⁻ ,X ⁻)	3.07	0.69	0.74	1.18	0.51	0.82	0.97	1.29	1.60	2.76
(Z ⁻ ,Y ⁻)	3.00	0.69	0.82	0.83	0.57	0.58	0.98	1.42	1.55	1.80
(X ⁻ ,Z ⁺)	3.17	0.65	0.45	1.07	0.31	0.74	0.96	1.45	1.80	2.02
(X ⁻ ,X ⁺)	3.06	0.71	0.70	0.94	0.48	0.65	1.01	1.26	2.50	2.42
(X ⁻ ,Y ⁺)	3.11	0.66	0.40	0.74	0.28	0.51	0.92	1.25	1.87	1.92
(X ⁻ ,Z ⁻)	3.08	0.73	0.67	1.08	0.46	0.74	0.97	1.26	1.96	2.38
(X ⁻ ,X ⁻)	3.04	0.70	0.62	0.90	0.43	0.62	0.99	1.36	2.07	2.01
(X ⁻ ,Y ⁻)	3.10	0.63	0.56	0.80	0.38	0.56	0.93	1.28	2.21	2.00
(Y ⁻ ,Z ⁺)	2.82	0.69	0.54	1.17	0.38	0.81	0.86	1.44	2.08	1.87
(Y ⁻ ,X ⁺)	2.82	0.76	0.63	0.99	0.44	0.69	0.86	1.24	2.26	2.02
(Y ⁻ ,Y ⁺)	2.81	0.74	0.51	1.33	0.35	0.92	0.87	1.24	2.16	2.83
(Y ⁻ ,Z ⁻)	2.73	0.71	0.65	1.06	0.45	0.73	0.82	1.26	2.36	1.84
(Y ⁻ ,X ⁻)	2.72	0.64	0.47	0.96	0.32	0.67	0.96	1.31	1.76	2.00
(Y ⁻ ,Y ⁻)	2.74	0.72	0.44	1.00	0.31	0.69	0.87	1.38	1.80	1.86

Table 1: Chosen parameters to characterize the resulting galaxy morphology of the two galaxies interactions with different orientations and rotations, The number on the left of each column has mass ratio 1:10 and the number on the right is for mass ratio 1:1.

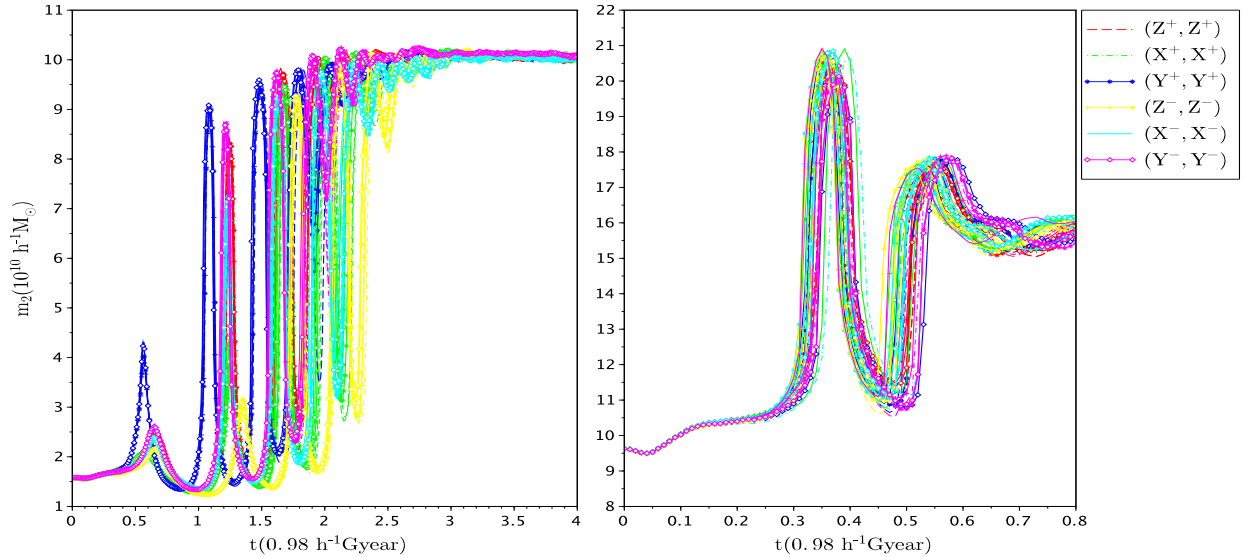


Figure 17: Comparison between mass ratios 1:10 (left) and 1:1 (right) of the evolution of the mass of the secondary galaxy, M_2 .

Figure 17 shows the evolution of the mass of the secondary galaxy. For the 1:10 cases the galaxy increases its mass steadily until the merger product includes most of the mass of the primary galaxy as well. In the 1:1 mass ratio cases there is a notable contraction of both galaxies visible in the simulation at $t \sim 0.35$ Gyr which brings greater mass within the radius used to measure the mass of the secondary galaxy. Then, the mass is reduced as the simulation progresses and the mass moves further away from the centre again. As one could expect, the dynamics of two equal galaxies evolves much faster than the evolution with two galaxies quite different in masses.

5 Discussions and conclusions

We have used the GADGET-2 N-body code to study the galaxy morphology and the time taken by two interacting galaxies (mass ratios 1:10 and 1:1 with the same bulge-to-disk ratios) to merge due to gravity. It was found that for case with a 1:10 mass ratio some interaction modes are grouped, with basically the same behavior for each group. These groups do not exist for case with galaxies of 1:1 mass ratio, where there is a unique group, and every case has almost the same evolution of distances between bulges and about the same merging time.

The evolution of the masses of each galaxy is completely different in both cases. For the case with a 1:10 mass ratio, the global maximum is located at the end evolution, meaning that the second galaxy increases its mass constantly. For the case with mass ratio 1:1, the global maximum is located around $t = 0.35$ Gyr, causing a reduction of the merging time. Of course, the galaxy morphology vary for each case due to the difference on masses since the dispersion of stars for the case 1:10 is bigger than the dispersion of stars in the case 1:1, for most of the interaction types.

The evolution of the galaxies is principally affected by the angular momentum of interaction of both galaxies, and secondly by rotation of the more massive galaxy. For a 1:10 mass ratio, the rotation can reduce or increase the merging time by an interval of ~ 0.9 ($0.98 \text{ h}^{-1} \text{ Gyr}$). In contrast, for the 1:1 mass ratio case, the relative rotation of galaxies can reduce or increase the merging time by an interval of ~ 0.2 ($0.98 \text{ h}^{-1} \text{ Gyr}$).

In all cases with 1:10 mass ratios and cases with the secondary galaxy with rotation and orientation Z^+ the merger product contains a disk in the $x - y$ plane, usually greatly extended with respect to the original primary disk both in radius and height, due to the high initial angular momentum about the z axis. The 1:10 mass ratio cases all take a long time to complete merging and produce a disk-like galaxy in all cases, in the plane of the original secondary orbit due to the high initial angular momentum in this plane. the disk is usually extended and distorted. During the interaction shell-like structures are formed in the plane of the final disk. though their formation from a companion with a tangential orbit contradicts the results of Karademir et al. (2019).

For the cases with equal masses the merging is more rapid and the disks less extended usually and the dstructures at intermediate times look more like parts of spiral arms. When the secondary galaxy is in the rotation state Z^+ the final product has a disturbed, asymmetric, warped disk, while Z^+, Z^+ has a box-peanut-like bulge. The other cases end in a bulge/ellipsoid-dominated galaxy (some box-peanut-like) due to the high initial angular momentum perpendicular to the $x - y$ plane.

Acknowledgements

We want to thank Dr. Iv nio Puerari and M.C. Diego Valencia En rriquez from INAOE institute in Tonantzintla, Puebla, M xico for their help teaching to one of us how to use GADGET-2 code.

References

- Bertin, G. 2000, Dynamics of Galaxies (Cambridge University Press)
- Besla G., Kallivayalil N., H. L. v. d. M. R. C. T. a. K. D. 2012, MNRS, 421, 2109
- Bode, P., Ostriker, J. P., & Turok, N. 2001, ApJ, 556, 93
- Bouwens, R., Cay n, L., & Silk, J. 1999, ApJ, 516, 77
- Boylan-Kolchin M., C.-P. M., & E., Q. 2008, MNRAS, 383, 93
- Burkert, A. T. J. W., Truran, J. W., & Hensler, G. 1992, ApJ, 391, 651
- Daylan, T., Finkbeiner, D. P., Hooper, D., et al. 2016, PDU, 12, 1
- Dwek, E., Arendt, R., Hauser, M., et al. 1995, ApJ, 445, 716
- Gallagher III, J. S., & Ostriker, J. P. 1972, AJ, 77, 288
- Giallongo, E., Menci, N., Poli, F., D’Odorico, S., & Fontana, A. 2000, ApJL, 530, L73
- Holtzman, J. A., Watson, A. M., Baum, W. A., et al. 1998, AJ, 115, 1946
- Hopkins P.F., Cox T.J., H. L. N. D. H. C. a. M. N. 2013, MNRS, 430, 1901
- Iverson, R. J., Smail, I., Papadopoulos, P. P., et al. 2010, MNRAS, 404, 198
- Kacprzak, G. G., Churchill, C. W., Barton, E. J., & Cooke, J. 2011, ApJ, 733, 105
- Karademir, G. S., Remus, R.-S., Burkert, A., et al. 2019, MNRAS, 487, 318
- Kennicutt Jr., R. C. 1983, ApJ, 272, 54

- Kennicutt Jr., R. C., Roettiger, K. A., Keel, W. C., Van Der Hulst, J. M., & Hummel, E. 1987, *AJ*, 93, 1011
- Kim, C.-G., & Ostriker, E. C. 2018, *ApJ*, 853, 173
- Koyama, S. 2019, *ApJ*, 874, 142
- Larson, R. B., & Tinsley, B. M. 1978, *ApJ*, 219, 46
- Launhardt, R., Zylka, R., & Mezger, P. 2002, *A&A*, 384, 112
- Magorrian, J., Tremaine, S., Richstone, D., et al. 1998, *AJ*, 115, 2285
- Milosavljević, M., & Merritt, D. 2001, *ApJ*, 563, 34
- Moody C.E., Romanowsky A.J., C. T. N. G., & J.R., P. 2014, *MNRS*, 444, 1475
- Moreno, J., Torrey, P., Ellison, S. L., et al. 2019, *MNRAS*, 485, 1320
- Oppenheimer, B. R., Hambly, N. C., Digby, A. P., Hodgkin, S. T., & Saumon, D. 2001, *Sci*, 292, 698
- Paul, S. and John, R. S., & Gupta, P. and Kumar, H. 2017, *MNRAS*, 471, 2
- Pontzen, A., Tremmel, M., Roth, N., et al. 2016, *MNRAS*, 465, 547
- Rose, R. D., Parker, H. M., Lowry, R. A., Kuhlthau, A. R., & Beams, J. W. 1969, *PhRvL*, 23, 655
- Salviander, S., Shields, G. A., Gebhardt, K., & Bonning, E. W. 2007, *ApJ*, 662, 131
- Springel, V. 2005, *MNRAS*, 364, 1105
- Springel, V., Di Matteo, T., & Hernquist, L. 2005, *MNRAS*, 361, 776
- Springel, V., & White, S. D. 1999, *MNRAS*, 307, 162
- Turner, E. L. 1976, *ApJ*, 208, 20
- van der Kruit, P. 2010, in *Galaxies and their Masks* (Springer), 153–168
- Voit, G. M. 2005, *RvMP*, 77, 207
- Wallin, J., Holincheck, A., & Harvey, A. 2016, *A&C*, 16, 26
- Wechsler, R. H., & Tinker, J. L. 2018, *ARA&A*, 56, 435
- Wuyts S., Franx M., C. T., & N.M.F., S. 2009, *AJ*, 700, 799
- Xu, B.-X., Wu, X.-B., & Zhao, H.-S. 2007, *ApJ*, 664, 198